Anisotropic spontaneous curvatures in lipid membranes

Nikhil Walani, Jennifer Torres, and Ashutosh Agrawal*
Department of Mechanical Engineering, University of Houston, Houston, Texas 77004, USA
(Received 20 September 2013; revised manuscript received 7 March 2014; published 26 June 2014)

Symmetry restrictions due to fluidity require the strain energy in the Helfrich theory of lipid membranes to be locally isotropic in nature. Although this framework is suitable for modeling the interaction of membranes with proteins that generate spherical curvature such as clathrin, there are other important membrane-bending proteins such as BIN-amphiphysin-Rvs proteins that form a cylindrical coat with different curvatures in the longitudinal and the circumferential directions. In this work, we present a detailed mathematical treatment of the theory of lipid membranes incorporating anisotropic spontaneous curvatures. We derive the associated Euler-Lagrange equations and the edge conditions in a generalized setting that allows spatial heterogeneities in the properties of the membrane-protein system. We employ this theory to model the constriction of a membrane tubule by a cylindrical scaffold. In particular, we highlight the role of the equilibrium equation in the tangential plane in regulating the spatial variation of the surface tension field.

DOI: 10.1103/PhysRevE.89.062715 PACS number(s): 87.16.ad, 87.10.Pq, 87.16.dm, 87.15.kt

I. INTRODUCTION

Cellular membranes undergo dynamic remodeling for successful execution of various processes such as cellular transport, cell mobility, and cell division, to name a few [1–6]. This in general entails local bending of the membrane that could single handedly or collectively be caused by (i) curvature-inducing proteins or lipids, (ii) active force-generating cytoskeletal filaments, and (iii) symmetry-breaking enzymes [5,6]. In the existing literature on membrane mechanics, this bending effect has been modeled on the continuum scale by introducing a so-called spontaneous curvature field. The application of this concept has ranged from studies modeling shapes of biological structures such as red blood cells to studies modeling processes such as cellular transport [1,3].

The idea of a spontaneous curvature field is tied to the form of the strain energy function of a lipid membrane. For the Helfrich model, the strain energy depends on the local mean curvature and the Gaussian curvature of the surface [7–9]. This was rigorously proven on the basis of symmetry restrictions that ensure membranes offer vanishing resistance to in-plane shear deformations as they behave like two-dimensional fluids [10,11]. For the classical Helfrich model with quadratic dependence on mean curvature and linear dependence on Gaussian curvature, a preferred geometry imposed by curvature-inducing proteins can be generated by prescribing a resting mean curvature and a Gaussian curvature. In general, the preferred mean curvature, called the spontaneous curvature, has been used in the literature to regulate the membrane geometry by shifting the vertex of the parabolic energy landscape (associated with the mean curvature) to the prescribed curvature.

This approach works well for proteins that form spherical coats and induce an isotropic curvature. One excellent example of such a protein is clathrin, which plays an important role in the various vesicle-mediated transport processes in cells [2,3]. However, there is a different set of curvature-inducing proteins called the BIN-amphiphysin-Rvs (BAR) proteins that generate a cylindrical curvature instead of a spherical curvature [12–15]. Figure 1 shows the two types of protein scaffolds and their effect on membrane geometry. As the normal curvatures along the longitudinal axis and the circumferential direction of a cylinder are different, spontaneous curvatures generated by such proteins are anisotropic in nature. As a consequence, the standard Helfrich model is not equipped to model such membrane-protein interactions because of the inherent isotropy built into the system.

To address this issue, several studies have proposed a modified quadratic strain energy in different contexts. A generalized energy for membranes where tilting and chirality of lipids give rise to anisotropic spontaneous curvatures was proposed in [16]. In a series of papers, the effect of anisotropic inclusions was studied via a mismatch tensor that energetically penalized the difference between the intrinsic curvatures preferred by the inclusions and the local membrane curvatures along the preferred directions [17–19]. For a nematic membrane made of rodlike molecules, a strain energy that incorporated spontaneous curvatures in both the normal curvatures and the twist was proposed in [20]. Models for BAR protein attachment that account for membrane-protein electrostatic interactions and symmetry breaking by loop insertion have been reviewed in [21]. In addition to these works, computational models and an all-atom molecular dynamics model have been developed to investigate the interaction of BAR proteins with the lipid membrane [22–29]. For an extensive list of theoretical and computational studies on membrane-protein interactions, we refer the reader to [30,31].

In this paper we build upon these works to present a detailed derivation of a generalized theory to model interactions of a membrane with nonspherical protein scaffolds. In particular, we derive the Euler-Lagrange equations in a fully nonlinear setting for an inhomogeneous membrane that is equipped to capture spatial variations in membrane and protein coat properties. In addition to the *modified shape equation*, we present the force equilibrium equation in the tangential plane in the context of anisotropic membranes. Furthermore, we derive the explicit expressions for forces and moment that act locally at any arbitrary boundary in such a membrane. The paper is organized as follows. In Sec. II we discuss the strain

*Corresponding author: aagrawa4@central.uh.edu

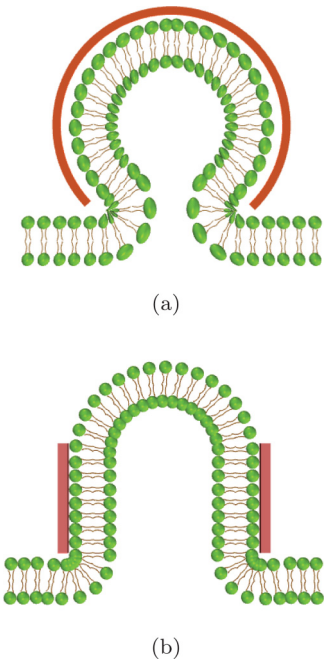

FIG. 1. (Color online) Different types of protein scaffolds around the membrane (shown in red): (a) a spherical scaffold made by proteins such as clathrin and (b) a cylindrical scaffold such as those made by BAR proteins.

energy function for a membrane with anisotropic curvatures. In Sec. III we compute the variations and derive the Euler-Lagrange equations and the edge conditions. In Sec. IV we customize the governing equations for axisymmetric surfaces and model the interactions of a cylinder and a spherical vesicle with crescent-shaped proteins. Finally, we summarize our results in Sec. V.

II. STRAIN ENERGY

The lipid membrane and the protein scaffold form a nonstandard composite system. It bears similarity to fiber-reinforced solid materials that exhibit anisotropy generated by the directionality of the fibers [32]. However, there is a fundamental difference that distinguishes the two materials. In a fiber-reinforced material, the fibers are embedded in the matrix and as a result, the fibers get convected with the matrix when subjected to a deformation. In contrast, BAR proteins are not transmembrane proteins and sit outside the outer monolayer. Thus, while the protein shell is more solidlike, the membrane inside still remains fluid, allowing lipids to diffuse over the surface. Furthermore, the curvature-inducing proteins are more dynamic and can diffuse and reorient on the surface and self-assemble in different configurations depending on their spatial distribution and membrane geometry. As a result, these proteins cannot be modeled as embedded entities that get convected with a deforming membrane. This fact limits the use of symmetry arguments in a reference configuration typically used to obtain restrictions on the constitutive functions of fiber-reinforced materials. To circumvent this problem, we impose symmetry restrictions in the current configuration, similar to the approach proposed in [17–19]. This ensures incorporation of directional effects from the curvature-inducing

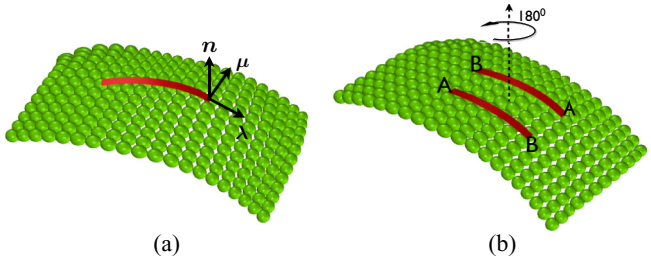

(a) (b)

FIG. 2. (Color online) Protein attachment on the membrane: (a) orientation of the protein in the tangential plane and (b) 180° rotation of the protein about the surface normal leads to an indistinguishable state.

proteins without picking up unphysical effects due to protein embedding.

Let ω be a two-dimensional surface with a nonuniform distribution of crescent-shaped bar proteins that tend toward anisotropic curvatures. The locus of points on ω is tracked by the position vector $\mathbf{r}(\theta^\mu)$, where θ^μ $(\mu = 1,2)$ are the surface coordinates. Here and henceforth, greek indices range over $\{1,2\}$ and, if repeated, are summed over that range. The basis vectors on the tangential plane at any point are given by $\mathbf{a}_\alpha = \mathbf{r}_{,\alpha}$, where $(\,)_{,\alpha} = \partial(\,)/\partial\theta^\alpha$. This yields the metric $a_{\alpha\beta} = \mathbf{a}_\alpha \cdot \mathbf{a}_\beta$ and the unit surface normal vector $\mathbf{n} = \mathbf{a}_1 \times \mathbf{a}_2 / |\mathbf{a}_1 \times \mathbf{a}_2|$. The local curvature tensor field is given by $\mathbf{b} = b_{\alpha\beta}\mathbf{a}^\alpha \otimes \mathbf{a}^\beta$, where

$$b_{\alpha\beta} = \mathbf{n} \cdot \mathbf{r}_{,\alpha\beta} = -\mathbf{a}_\alpha \cdot \mathbf{n}_{,\beta} \tag{1}$$

are the coefficients of the second fundamental form, $\mathbf{a}^\alpha = a^{\alpha\beta}\mathbf{a}_\beta$ are the contravariant basis vectors, and $(a^{\alpha\beta}) = (a_{\alpha\beta})^{-1}$ is the dual metric [33].

We assume that the curvatures induced by the proteins depend on both the geometry of the proteins and their local concentrations. The orientation of a protein on the surface is given by a unit vector $\boldsymbol{\lambda}(\theta^\mu)$ that is tangential to the one-dimensional curve that captures the in-plane protein geometry as shown in Fig. 2(a). The orientational vector $\boldsymbol{\lambda}$ and the surface normal $\mathbf{n}$ furnish a third orthonormal vector $\boldsymbol{\mu} = \mathbf{n} \times \boldsymbol{\lambda}$, which together form a local triad $\{\boldsymbol{\lambda}, \boldsymbol{\mu}, \mathbf{n}\}$ at any point on the surface.

Since a membrane behaves as a fluid shell offering bending resistance, the strain energy function depends on the curvature tensor $\mathbf{b}$. However, unlike the classical model, for the present case we assume an additional dependence on a structural tensor

$$\mathbf{M} = \boldsymbol{\lambda} \otimes \boldsymbol{\lambda} - \boldsymbol{\mu} \otimes \boldsymbol{\mu} \tag{2}$$

to capture the anisotropic spontaneous curvatures generated from membrane-protein interactions. Such a structural tensor is routinely used to define orthotropic symmetry in two-dimensional materials [34]. In the present setting, we do not resort to a reference configuration and require the model to have orthotropic symmetry in the current configuration. This is motivated by the fact that a crescent-shaped protein rotated by 180° cannot be distinguished from the original protein. As a consequence, the normal spontaneous curvatures they generate are also indistinguishable [Fig. 2(b)]. As is necessary for any material, we require the strain energy density $W(\mathbf{b},\mathbf{M})$ to be Galilean invariant. This yields a list of invariants

$$I = \{\mathrm{tr}(\mathbf{b}), \mathrm{tr}(\mathbf{M}), \det(\mathbf{b}), \det(\mathbf{M}), \mathrm{tr}(\mathbf{Mb})\}. \tag{3}$$

Since the second and fourth invariants above are constant scalar fields, the irreducible basis comprises three elements H, K, and D, where $H = \mathrm{tr}(\mathbf{b})/2$ is the mean curvature, $K = \det(\mathbf{b})$ is the Gaussian curvature, and $D = \mathrm{tr}(\mathbf{Mb})/2$ is the curvature deviator. In addition to H and K present in the Helfrich model, W now is dependent on a new element D because of the directionality imposed by an orthotropic protein scaffold.

To get insight into the invariants, we compute them in terms of the local principal curvatures. In the $\{\mathbf{a}_\alpha,\mathbf{a}_\beta\}$ and $\{\boldsymbol{\lambda},\boldsymbol{\mu}\}$ bases, they can be expressed as

$$H = \tfrac{1}{2}a^{\alpha\beta}b_{\alpha\beta} = (\kappa_\lambda + \kappa_\mu)/2, \tag{4a}$$

$$K = \tfrac{1}{2}\varepsilon^{\alpha\beta}\varepsilon^{\theta\psi}b_{\alpha\theta}b_{\beta\psi} = \kappa_\lambda\kappa_\mu - \tau^2, \tag{4b}$$

$$D = \tfrac{1}{2}b_{\alpha\beta}(\lambda^\alpha\lambda^\beta - \mu^\alpha\mu^\beta) = (\kappa_\lambda - \kappa_\mu)/2, \tag{4c}$$

where

$$\kappa_\lambda = b_{\alpha\beta}\lambda^\alpha\lambda^\beta, \quad \kappa_\mu = b_{\alpha\beta}\mu^\alpha\mu^\beta, \quad \tau = b_{\alpha\beta}\lambda^\alpha\mu^\beta \tag{5}$$

are the normal curvatures along $\boldsymbol{\lambda}$, $\boldsymbol{\mu}$, and the twist, respectively. Above, λ^α and μ^α are the projections of $\boldsymbol{\lambda}$ and $\boldsymbol{\mu}$ along the tangential vectors with

$$\begin{aligned}\lambda^\alpha &= \boldsymbol{\lambda}\cdot\mathbf{a}^\alpha,\\ \mu^\alpha &= \boldsymbol{\mu}\cdot\mathbf{a}^\alpha = (\mathbf{n}\times\boldsymbol{\lambda})\cdot\mathbf{a}^\alpha = \varepsilon^{\theta\alpha}\lambda^\psi a_{\theta\psi},\end{aligned} \tag{6}$$

where $\varepsilon^{\alpha\beta} = a^{-1/2}e^{\alpha\beta}$, $a = \det(a_{\alpha\beta})$, and $e^{\alpha\beta}$ is the permutation tensor with $e^{12} = -e^{21} = 1$ and zero if $\alpha = \beta$. From Eq. (4c) it is evident that D is the difference in the normal curvatures along the two orthogonal directions allowing us to prescribe a new spontaneous curvature D_0 that captures the protein-induced anisotropic curvatures. This is similar to prescribing H_0, the spontaneous curvature associated with the mean curvature in the Helfrich model. Since $\{H,D\}$ together uniquely determine $\{\kappa_\lambda,\kappa_\mu\}$ and vice versa [see Eq. (4)], prescribing $\{H_0,D_0\}$ is analogous to imposing preferred curvatures $\{\kappa_\lambda^0,\kappa_\mu^0\}$ in the two directions $\boldsymbol{\lambda}$ and $\boldsymbol{\mu}$. In contrast, imposing a set of $\{H_0,K_0\}$ can lead to infinitely many combinations of $\{\kappa_\lambda^0,\kappa_\mu^0\}$. Hence, the unique direction of attaching proteins cannot be deciphered in a model that depends solely on H and K.

III. VARIATIONS

The integration of the strain energy per unit area over the entire surface ω gives the total strain energy

$$\tilde{E} = \int_\omega W(H,D,K;\theta^\alpha). \tag{7}$$

An explicit dependence on surface coordinates allows modeling of heterogeneous membranes with spatially varying properties [35]. To impose the area and the volume constraints, we obtain an augmented potential energy functional

$$E = \int_\omega [W(H,D,K;\theta^\alpha) + \lambda(\theta^\alpha)]da - pV(\omega), \tag{8}$$

where $\lambda(\theta^\alpha)$ is the surface tension field and p is the transmembrane pressure [36]. We allow tension to vary spatially in order to prevent local areal dilation. This assumption is based on the observation that a bilayer can only endure a maximum of 2%–3% stretch before tearing apart [37].

We consider a family of surfaces generated by $\mathbf{r}(\theta^\alpha;\epsilon)$. The virtual displacement of the surface is given by $\mathbf{u}(\theta^\alpha) = \frac{\partial}{\partial\epsilon}\mathbf{r}(\theta^\alpha;\epsilon)|_{\epsilon=0} = \dot{\mathbf{r}}$, where the superposed dot refers to the derivative with respect to the parameter ϵ [38]. Variation of E in Eq. (8) yields

$$\dot{E} = \int_\omega \dot{W}da + \int_\omega (W+\lambda)(\dot{J}/J)\,da - p\dot{V}, \tag{9}$$

where $J = \sqrt{a/A}$ is the ratio of the material area after deformation to that before and

$$\dot{W} = W_H\dot{H} + W_K\dot{K} + W_D\dot{D}. \tag{10}$$

The variations of the mean curvature and the Gaussian curvature were derived in [38] and are given by

$$2\dot{H} = a^{\alpha\beta}\dot{b}_{\alpha\beta} - b^{\alpha\beta}\dot{a}_{\alpha\beta}, \tag{11a}$$

$$\dot{K} = -Ka^{\alpha\beta}\dot{a}_{\alpha\beta} + \tilde{b}^{\alpha\beta}\dot{b}_{\alpha\beta}. \tag{11b}$$

In this paper we focus on the variation of the curvature deviator, which, with the help of Eq. (4c), can be expressed as

$$\dot{D} = \tfrac{1}{2}(\dot{\kappa_\lambda} - \dot{\kappa_\mu}). \tag{12}$$

Using Eq. (5), variations of κ_λ and κ_μ can be expressed as

$$\begin{aligned}\dot{\kappa_\lambda} &= \dot{b}_{\alpha\beta}\lambda^\alpha\lambda^\beta + 2b_{\alpha\beta}\dot{\lambda}^\alpha\lambda^\beta,\\ \dot{\kappa_\mu} &= \dot{b}_{\alpha\beta}\mu^\alpha\mu^\beta + 2b_{\alpha\beta}\dot{\mu}^\alpha\mu^\beta.\end{aligned} \tag{13}$$

From Eq. (6) and the relation $\mathbf{a}^\alpha = a^{\alpha\gamma}\mathbf{a}_\gamma$, we can compute

$$\dot{\lambda}^\alpha = a^{\alpha\gamma}(\boldsymbol{\lambda}\cdot\dot{\mathbf{a}}_\gamma) + (\boldsymbol{\lambda}\cdot\mathbf{a}_\gamma)\dot{a}^{\alpha\gamma}, \tag{14a}$$

$$\dot{\mu}^\alpha = (\dot{\mathbf{n}}\times\boldsymbol{\lambda})\cdot\mathbf{a}^\alpha + (\mathbf{n}\times\boldsymbol{\lambda})\cdot\dot{\mathbf{a}}^\alpha. \tag{14b}$$

It is important to emphasize that in the current model $\boldsymbol{\lambda}$ is prescribed *a priori*. As a result, it is unaffected by the virtual displacements and $\dot{\boldsymbol{\lambda}} = \mathbf{0}$. However, since $\boldsymbol{\mu} = \mathbf{n}\times\boldsymbol{\lambda}$, $\dot{\boldsymbol{\mu}} \neq \mathbf{0}$ because of the variations of $\mathbf{n}$. Since $\mathbf{n}\cdot\mathbf{n} = 1$, $\dot{\mathbf{n}}$ is perpendicular to $\mathbf{n}$ and lies in the tangential plane. As a result, $\dot{\mathbf{n}}\times\boldsymbol{\lambda}$ is oriented along the normal whose projection in the tangential plane vanishes. This simplifies Eq. (14b) to

$$\dot{\mu}^\alpha = a^{\alpha\gamma}(\boldsymbol{\mu}\cdot\dot{\mathbf{a}}_\gamma) + (\boldsymbol{\mu}\cdot\mathbf{a}_\gamma)\dot{a}^{\alpha\gamma}. \tag{15}$$

Substituting Eqs. (13), (14a), and (15) in (12), we can finally obtain

$$\begin{aligned}\dot{D} = {} & \tfrac{1}{2}\dot{b}_{\alpha\beta}(\lambda^\alpha\lambda^\beta - \mu^\alpha\mu^\beta) + b_{\alpha\beta}[a^{\alpha\gamma}\dot{\mathbf{a}}_\gamma\cdot(\lambda^\beta\boldsymbol{\lambda} - \mu^\beta\boldsymbol{\mu})\\ & + \dot{a}^{\alpha\gamma}\mathbf{a}_\gamma\cdot(\lambda^\beta\boldsymbol{\lambda} - \mu^\beta\boldsymbol{\mu})].\end{aligned} \tag{16}$$

A. Tangential variations

For tangential variation $\mathbf{u} = u^\lambda\mathbf{a}_\lambda$, we can show (see [38] for details)

$$\dot{\mathbf{a}}_\gamma = u^\eta{}_{;\gamma}\mathbf{a}_\eta + u^\lambda b_{\lambda\gamma}\mathbf{n} \tag{17}$$

and

$$\dot{a}^{\alpha\gamma} = -a^{\alpha\theta}a^{\gamma\psi}(u_{\theta;\psi} + u_{\psi;\theta}). \tag{18}$$

Here and henceforth a semicolon signifies the covariant derivative along the tangential direction. Substitution of Eqs. (17)

and (18) in (14a) furnishes

$$\dot{\lambda}^{\alpha} = -\lambda_{\gamma} a^{\alpha\theta} a^{\gamma\psi} (u_{\theta;\psi} + u_{\psi;\theta}) + a^{\alpha\theta} u^{\gamma}_{;\theta} \lambda_{\gamma}. \tag{19}$$

Since the metric is covariant constant,

$$a^{\gamma\psi} u_{\psi;\theta} = u^{\gamma}_{;\theta}, \quad a^{\alpha\theta} u_{\theta;\psi} = u^{\alpha}_{;\psi}. \tag{20}$$

Combining Eqs. (19) with (20) yields

$$\dot{\lambda}^{\alpha} = -\lambda^{\psi} u^{\alpha}_{;\psi}. \tag{21}$$

Following a similar procedure, we can show

$$\dot{\mu}^{\alpha} = -\mu^{\psi} u^{\alpha}_{;\psi}. \tag{22}$$

We employ Eqs. (13), (21), and (22) along with the Mainardi-Codazzi equations and the variation of the covariant components of the curvature tensor [38]

$$\dot{b}_{\alpha\beta} = u^{\eta}_{;\alpha} b_{\eta\beta} + u^{\eta}_{;\beta} b_{\eta\alpha} + u^{\eta} b_{\eta\alpha;\beta} \tag{23}$$

to compute

$$\dot{\kappa}_{\lambda} = u^{\eta} b_{\alpha\beta;\eta} \lambda^{\alpha} \lambda^{\beta}, \quad \dot{\kappa}_{\mu} = u^{\eta} b_{\alpha\beta;\eta} \mu^{\alpha} \mu^{\beta}. \tag{24}$$

Substitution of Eq. (24) in Eq. (12) finally furnishes the variation of the curvature deviator

$$\dot{D} = u^{\eta} b_{\alpha\beta;\eta} (\lambda^{\alpha} \lambda^{\beta} - \mu^{\alpha} \mu^{\beta})/2. \tag{25}$$

Having obtained $\dot{D}$, we can now proceed to derive the force equilibrium equation in the tangential plane. Since $\dot{V}$ vanishes for tangential variations and $\dot{J}/J = u^{\eta}_{;\eta}$ [38], we can write Eq. (9) as

$$\dot{E} = \int_{\omega} [\dot{W} - u^{\eta}(W + \lambda)_{;\eta}] da + \int_{\omega} [u^{\eta}(W + \lambda)]_{;\eta} da, \tag{26}$$

where

$$W_{,\eta} = W_H H_{,\eta} + W_K K_{,\eta} + W_D D_{,\eta} + \partial W / \partial \theta^{\eta}. \tag{27}$$

Making use of $\dot{H} = u^{\eta} H_{,\eta}$ and $\dot{K} = u^{\eta} K_{,\eta}$ (derived in [38]) together with Eqs. (10) and (25)–(27) and the Stokes theorem, we compute the Euler-Lagrange equation

$$\lambda_{,\eta} = -\partial W / \partial \theta^{\eta} - W_D [b_{\alpha\beta} (\lambda^{\alpha} \lambda^{\beta})_{;\eta}]. \tag{28}$$

The above equation allows for the computation of the surface tension field on the surface. It generalizes the tangential equilibrium equation derived in [11,38] for homogeneous membranes and in [35] for membranes interacting with isotropic curvature-inducing proteins. The first term on the right-hand side is a result of spatial heterogeneities in membrane properties and holds for both isotropic and anisotropic membranes. The second term is specific to anisotropic membranes and is governed by the functional dependence of the strain energy on D and the orientation of the proteins. If the membrane is homogeneous and isotropic, the right-hand side would vanish, furnishing a uniform surface tension over the entire surface. However, if the properties vary spatially or have a directionality, as is expected in the present context, the right-hand side can be nonzero, forcing the surface tension to evolve over the surface.

B. Normal variations

For normal variation $\mathbf{u} = u(\theta^{\alpha})\mathbf{n}$, we follow a similar procedure. Using Eqs. (14a) and (15) and the relations

$$\dot{\mathbf{a}}_{\alpha} = u_{,\alpha}\mathbf{n} - u b^{\beta}_{\alpha} \mathbf{a}_{\beta}, \quad \dot{a}_{\alpha\beta} = -2u b_{\alpha\beta}, \tag{29a}$$

$$\dot{b}_{\alpha\beta} = u_{;\alpha\beta} - u b_{\alpha\gamma} b^{\gamma}_{\beta} \tag{29b}$$

(see [38]), we derive

$$\dot{\lambda^{\alpha}} = u b^{\gamma}_{\psi} a^{\alpha\psi} \lambda_{\gamma}, \quad \dot{\mu^{\alpha}} = u b^{\gamma}_{\psi} a^{\alpha\psi} \mu_{\gamma}. \tag{30}$$

Substituting Eqs. (29b) and (30) in (13), we compute the variations of the normal curvatures

$$\dot{\kappa}_{\lambda} = \left[u_{;\alpha\beta} + u b_{\alpha\gamma} b^{\gamma}_{\beta}\right] \lambda^{\alpha} \lambda^{\beta},$$

$$\dot{\kappa}_{\mu} = \left[u_{;\alpha\beta} + u b_{\alpha\gamma} b^{\gamma}_{\beta}\right] \mu^{\alpha} \mu^{\beta}, \tag{31}$$

which together with Eq. (12) yield

$$\dot{D} = \left(u_{;\alpha\beta} + u b_{\alpha\gamma} b^{\gamma}_{\beta}\right) (\lambda^{\alpha} \lambda^{\beta} - \mu^{\alpha} \mu^{\beta})/2. \tag{32}$$

Substituting Eq. (32), along with the relations

$$2\dot{H} = \Delta u + u(4H^2 - 2K), \quad \dot{J}/J = -2Hu,$$

$$\dot{K} = 2KHu + (\tilde{b}^{\alpha\beta} u_{,\alpha})_{;\beta} \tag{33}$$

from [38] in Eq. (9) and employing the Stokes theorem, we compute the associated Euler-Lagrange equation

$$\tfrac{1}{2}[W_D(\lambda^{\alpha}\lambda^{\beta} - \mu^{\alpha}\mu^{\beta})]_{;\beta\alpha} + \tfrac{1}{2} W_D (\lambda^{\alpha}\lambda^{\beta} - \mu^{\alpha}\mu^{\beta}) b_{\alpha\gamma} b^{\gamma}_{\beta}$$
$$+\Delta\left(\tfrac{1}{2} W_H\right) + (W_K)_{;\beta\alpha} \tilde{b}^{\beta\alpha} + W_H(2H^2 - K)$$
$$+2H(K W_K - W) - 2H\lambda = p. \tag{34}$$

This is the modified *shape equation* in the context of anisotropic membranes. Suppressing the dependence of W on the curvature deviator D yields the original shape equation for the isotropic lipid membranes [11,35,36,38].

C. Edge conditions

With the Euler-Lagrange equations (28) and (34) satisfied, the variation of the energy E for a surface ω with a boundary $\partial\omega$ reduces to $\dot{E}_B = B_t + B_n$, where

$$B_t = \int_{\partial\omega} (W + \lambda) u^{\alpha} \nu_{\alpha} ds \tag{35}$$

and

$$B_n = \int_{\partial\omega} \Big\{ \tfrac{1}{2}(W_H - W_D) \nu^{\alpha} u_{,\alpha} - \tfrac{1}{2}[(W_H)_{,\alpha} - (W_D)_{,\alpha}] \nu^{\alpha} u$$
$$+ (W_K \tilde{b}^{\alpha\beta} + W_D \lambda^{\alpha} \lambda^{\beta}) \nu_{\beta} u_{,\alpha}$$
$$- [(W_K)_{,\alpha} \tilde{b}^{\alpha\beta} + (W_D \lambda^{\alpha} \lambda^{\beta})_{;\alpha}] \nu_{\beta} u \Big\} ds. \tag{36}$$

Equation (35) is the contribution from the tangential variations, which remains the same as that for the isotropic case [36]. In contrast, the contribution from the normal variations given by Eq. (36) is altered by the inclusion of the curvature deviator.

We define a vector $\boldsymbol{\tau}$ as the unit tangent to $\partial\omega$ as shown in Fig. 3 by taking the derivative with respect to the arc length parametrizing the boundary $\partial\omega$, $\boldsymbol{\tau} = \frac{d\mathbf{r}[\theta^{\alpha}(s)]}{ds}$. The unit normal to the boundary lying in the tangent plane to the surface can then be defined by the vector $\boldsymbol{\nu} = \boldsymbol{\tau} \times \mathbf{n}$. Using the orthonormality of $\boldsymbol{\nu}$ and $\boldsymbol{\tau}$, we can decompose the derivatives

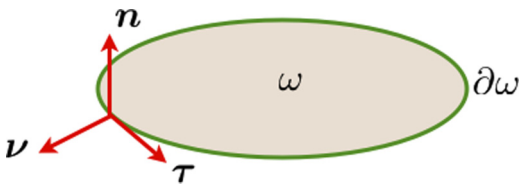

FIG. 3. (Color online) Three orthonormal vectors on a boundary $\partial\omega$.

$u_{,\alpha}$ in Eq. (36) as $u_{,\alpha} = \tau_\alpha u' + \nu_\alpha u_{,\nu}$, where u' is the derivative along $\boldsymbol{\tau}$ in the direction of increasing arc length and $u_{,\nu}$ is the normal derivative along $\boldsymbol{\nu}$ [36]. We combine this with $u_{,\nu} = -\boldsymbol{\tau}\cdot\boldsymbol{\omega} - (\kappa_\nu \boldsymbol{\nu} + \tau\boldsymbol{\tau})\cdot\mathbf{u}$ and $u = \mathbf{u}\cdot\mathbf{n}$ to recast the edge contributions for a piecewise smooth boundary as

$$\dot{E}_B = \int_{\partial\omega} (F_\nu \boldsymbol{\nu} + F_\tau \boldsymbol{\tau} + F_n \mathbf{n})\cdot\mathbf{u}\, ds - \int_{\partial\omega} M\boldsymbol{\tau}\cdot\boldsymbol{\omega} ds + \sum_i \mathbf{f}_i\cdot\mathbf{u}_i, \tag{37}$$

where

$$\begin{aligned} M &= \tfrac{1}{2}W_H + \kappa_\tau W_K + W_D\lambda^\alpha\lambda^\beta\nu_\beta\nu_\alpha - \tfrac{1}{2}W_D,\\ F_\nu &= W + \lambda - \kappa_\nu M,\\ F_\tau &= -\tau M,\\ F_n &= (\tau W_K)' - \tfrac{1}{2}(W_H)_{,\nu} - (W_K)_{,\beta}\tilde{b}^{\alpha\beta}\nu_\alpha\\ &\quad + \tfrac{1}{2}(W_D)_{,\nu} - (W_D\lambda^\alpha\lambda^\beta)_{;\beta}\nu_\alpha - (W_D\lambda^\alpha\lambda^\beta\nu_\beta\tau_\alpha)',\\ \mathbf{f}_i &= (W_K[\tau] + W_D[\lambda^\alpha\lambda^\beta\nu_\beta\tau_\alpha])_i\mathbf{n}. \end{aligned} \tag{38}$$

Square brackets indicate forward jumps in values within the brackets at the corners of the boundary, where there is a jump in $\boldsymbol{\tau}$. Above, M is the bending moment per unit length, F_ν is the in-plane normal force per unit length, F_τ is the in-plane shear force per unit length, F_n is the transverse shear force per unit length and $\mathbf{f}_i$ is the force applied at ith corner of $\partial\omega$. As expected, the anisotropic contribution to the strain energy results in modified expressions for the boundary forces and moment, furnishing an extension to the edge conditions derived for isotropic membranes [39–42].

IV. EXAMPLE

In this section we test the proposed theory by simulating the constriction of a cylindrical tubule by an exterior scaffold made of crescent-shaped proteins, such as BAR protein dimers. To this end, we customize the equations derived in the previous section for axisymmetric surfaces parametrized by meridional arc length s and azimuthal angle θ. For such a surface,

$$\mathbf{r}(s,\theta) = r(s)\mathbf{e}_r(\theta) + z(s)\mathbf{k}, \tag{39}$$

where $r(s)$ is the radius from axis of revolution, $z(s)$ is the elevation from a base plane, and $(\mathbf{e}_r,\mathbf{e}_\theta,\mathbf{k})$ form the coordinate basis. Since $(r')^2 + (z')^2 = 1$, we can define an angle ψ such that

$$r'(s) = \cos\psi, \quad z'(s) = \sin\psi. \tag{40}$$

Above and in the rest of the section, $()' = \partial()/\partial s$. With $\theta^1 = s$ and $\theta^2 = \theta$, we can easily show that

$$\mathbf{a}_1 = r'\mathbf{e}_r + z'\mathbf{k}, \quad \mathbf{a}_2 = r\mathbf{e}_\theta, \qquad \mathbf{n} = -\sin(\psi)\mathbf{e}_r + \cos(\psi)\mathbf{k}. \tag{41}$$

Using Eq. (41) and its derivative, we can show that the metric $(a_{\alpha\beta}) = \mathrm{diag}(1,r^2)$, the dual metric $(a^{\alpha\beta}) = \mathrm{diag}(1,\frac{1}{r^2})$, and the covariant components of the curvature tensor $(b_{\alpha\beta}) = \mathrm{diag}(\psi',r\sin\psi)$. Together they furnish the two invariants

$$2H = \psi' + \frac{\sin\psi}{r}, \tag{42a}$$

$$K = H^2 - [H - (\sin\psi)/r]^2. \tag{42b}$$

The BAR proteins align in a helical pattern on the membrane tubule [14]. The lateral and tip to tip interactions between the dimers help to deform the underlying membrane [27]. To achieve this efficiently, the BAR proteins maintain close proximity and orient themselves on the cylindrical surface with low tilt angle [13] (tilt with respect to the longitudinal axis of the tubule). Thus, for our simulations, we neglect the small tilt angle and assume a continuous distribution of crescent-shaped dimers aligned in the circumferential direction. As a result, the two orientation vectors are given by

$$\boldsymbol{\lambda} = -\mathbf{e}_\theta, \quad \boldsymbol{\mu} = \cos\psi\,\mathbf{e}_r + \sin\psi\,\mathbf{k}. \tag{43}$$

The corresponding normal curvatures in the two directions become $\kappa_\lambda = (\sin\psi)/r$ and $\kappa_\mu = \psi'$. Together, they yield the curvature deviator $D = [(\sin\psi)/r - \psi']/2$.

We consider an extension of the Helfrich energy W that is quadratic in the mean curvature H and the curvature deviator D. For the time being, we suppress the dependence of W on the Gaussian curvature K as the influence of protein coat on the Gaussian modulus is not yet known. We discuss the possible consequences of different Gaussian moduli in Sec. IV A. The generalized form of W can therefore be written as

$$W(H,D;s) = \hat{k}_1(s)[H - H_0(s)]^2 + \hat{k}_2(s)[D - D_0(s)]^2 + 2\hat{k}_{12}(s)[H - H_0(s)][D - D_0(s)], \tag{44}$$

where $H_0(s)$ and $D_0(s)$ are the preferred H and D values that arise because of the anisotropic curvatures generated by the protein scaffold. In addition to the spontaneous curvatures, we assume that the protein scaffold also alters the effective bending moduli and hence allows them to vary spatially. In the absence of the protein coat, the last two terms vanish, furnishing the standard Helfrich energy. To get some additional insight into the membrane-protein system, we can express the above energy in terms of the normal curvatures in the $\boldsymbol{\lambda}$ and $\boldsymbol{\mu}$ directions in lieu of the mean curvature and the curvature deviator. With the help of Eqs. (4a) and (4c), Eq. (44) can be written as

$$W = k_1(s)\left[\kappa_\lambda - \kappa_\lambda^0(s)\right]^2 + k_2(s)\left[\kappa_\mu - \kappa_\mu^0(s)\right]^2 + 2k_{12}(s)\left[\kappa_\lambda - \kappa_\lambda^0(s)\right]\left[\kappa_\mu - \kappa_\mu^0(s)\right]. \tag{45}$$

The link between the Eqs. (44) and (45) is provided by the relations

$$\begin{aligned} &\hat{k}_1 = k_1 + k_2 + 2k_{12}, \quad \hat{k}_2 = k_1 + k_2 - 2k_{12},\\ &\hat{k}_{12} = (k_1 - k_2),\\ &H_0 = \left(\kappa_\lambda^0 + \kappa_\mu^0\right)/2, \quad D_0 = \left(\kappa_\lambda^0 - \kappa_\mu^0\right)/2. \end{aligned} \tag{46}$$

In Eq. (45), $\{\kappa_\lambda^0,\kappa_\mu^0\}$ and $\{k_1,k_2\}$ are the spontaneous curvatures and the bending moduli along the directions $\boldsymbol{\lambda}$ and $\boldsymbol{\mu}$ and hence

provide a more intuitive picture of the effect of the protein scaffold on the membrane in the two directions.

The shape equation (34) for $W(H,D;s)$ and axisymmetric geometry reduces to

$$p = \frac{L'}{r} + W_H(2H^2 - K) - 2H(W + \lambda - W_D D) + \frac{(W_D)'\cos\psi}{r}, \tag{47}$$

where

$$L/r = \tfrac{1}{2}[(W_H)' - (W_D)']. \tag{48}$$

The equilibrium equation in the tangential plane [Eq. (28)] takes the form

$$\lambda' = -W'. \tag{49}$$

We account for the area incompressibility of the membrane by transforming the independent variable from arc length s to area a employing the relation $da/ds = 2\pi r$. In addition, we nondimensionalize the system of equations and define

$$\bar{r} = r/R_0, \quad \bar{z} = z/R_0, \quad \bar{a} = a/2\pi R_0^2, \quad \bar{\kappa}_\lambda = R_0\kappa_\lambda,$$
$$\bar{\kappa}_\mu = R_0\kappa_\mu, \quad \bar{H} = R_0 H, \quad \bar{D} = R_0 D, \quad \bar{\lambda} = \lambda R_0^2/k_0,$$
$$\bar{L} = R_0 L/k_0, \quad \bar{k}_1 = \hat{k}_1/k_0, \quad \bar{k}_2 = \hat{k}_2/k_0,$$
$$\bar{k}_{12} = \hat{k}_{12}/k_0, \tag{50}$$

where R_0 is a reference radius of curvature and k_0 is the bending modulus of the uncoated membrane.

The uncoated tubule has a uniform circumferential radius ($\bar{\kappa}_\lambda = 0.5$) with $\bar{k}_1 = 1$, $\bar{k}_2 = \bar{k}_{12} = 0$, and $\kappa_\lambda^0 = \kappa_\mu^0 = 0$. We simulate the shape evolution of the tubule for a sequence of nonuniform protein concentrations (C_1, C_2, C_3) shown in Fig. 4(a). In a realistic setting, such a changing spatial concentration would correspond to a binding-driven accumulation of the protein dimers. Since in the present study we do not explicitly model the self-assembly dynamics of dimers, we prescribe the protein concentration field *a priori*. We cap the concentration to a maximum value as the protein size and geometry would impose a physical restriction on the packing density. We assume that the effective membrane parameters influenced by the protein coat $(\bar{H}_0, \bar{D}_0, \bar{k}_1, \bar{k}_2)$ depend linearly on the protein concentration field [Fig. 4(b)]. A concentration-dependent preferred curvature has indeed been experimentally observed for the BAR domain attachments [12].

We assume that the protein scaffold prefers a narrower tubule and prescribe a larger curvature ($\bar{\kappa}_\lambda^0 = 1$) in the circumferential direction and zero curvature in the longitudinal direction ($\bar{\kappa}_\mu^0 = 0$). In the (H,D) framework, these maximum directional curvatures transform to $\bar{H}_0 = 0.5$ and $\bar{D}_0 = 0.5$. These values correspond to the maximum protein concentration and get scaled by the local concentration values in the rest of the coated domain. In addition, we assume that the protein coat results in increased effective bending modulus and set $\hat{k}_1 = 2$ and $\hat{k}_2 = 1$ in the highest concentration region. These parameters, computed from Eq. (46), assume a double stiffening of the membrane in the $\boldsymbol{\lambda}$ and $\boldsymbol{\mu}$ directions. This choice of parameters is in agreement with a stiffness of $20 \pm 10 k_B T$ for the BAR proteins computed by the shape-based coarse-graining approach [22].

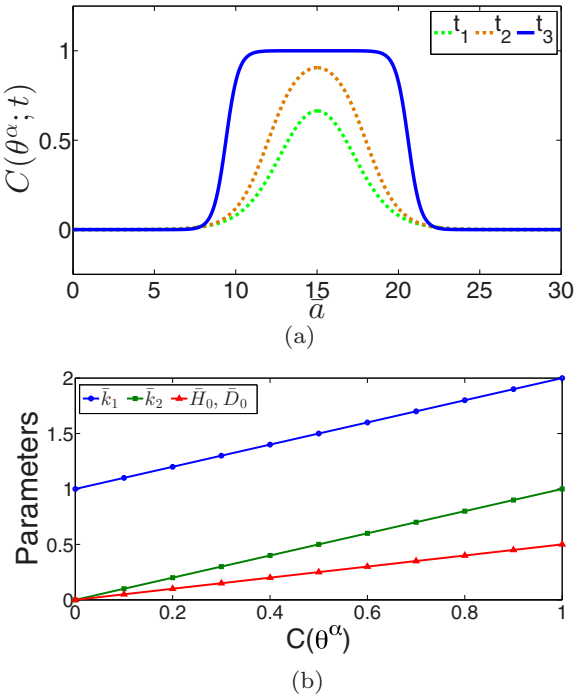

FIG. 4. (Color online) (a) Three prescribed spatially varying protein concentration fields and (b) linear dependence of the various protein-induced parameters on the concentration values.

For the above-mentioned parameters, we solve the differential equations (40), (42a), and (47)–(49) over an area domain varying from 0 to $\bar{a}_0 = 30$ for vanishing transmembrane pressure subject to the boundary conditions

$$\bar{r}(0) = 2, \quad \bar{z}(0) = 0, \quad \psi(0) = \pi/2,$$
$$\bar{r}(\bar{a}_0) = 2, \quad \psi(\bar{a}_0) = \pi/2, \quad \bar{\lambda}(\bar{a}_0) = 1/16. \tag{51}$$

The last boundary condition is obtained from the solution of the standard shape equation to maintain the original cylindrical geometry far away from the protein coat domain.

The computed tubule geometry and the surface tension field are shown in Fig. 5. As the protein coat continues to grow, the preferred circumferential and meridional curvatures are effectively imposed and the tubule attains a smaller radius in the coated domain [Fig. 5(a)]. It is important to note that the changes in the geometry are accompanied by a concomitant change in the surface tension values shown in Fig. 5(b). The surface tension profile closely follows the concentration profile. From a far away normalized resting tension of 0.06, the surface tension increases to 0.27 in the protein coat domain (for C_3 concentration field), leading to an approximate increase by 450%. Such a drastic change in the surface tension would be specifically relevant to comprehend the role and energetics of fission proteins that form cylindrical coats. The role of the tangential equilibrium equation in capturing the spatial variation in the surface tension thus cannot be undermined.

A. Effect of Gaussian modulus

In the results presented so far, we had suppressed the role of Gaussian energy because of lack of experimental or

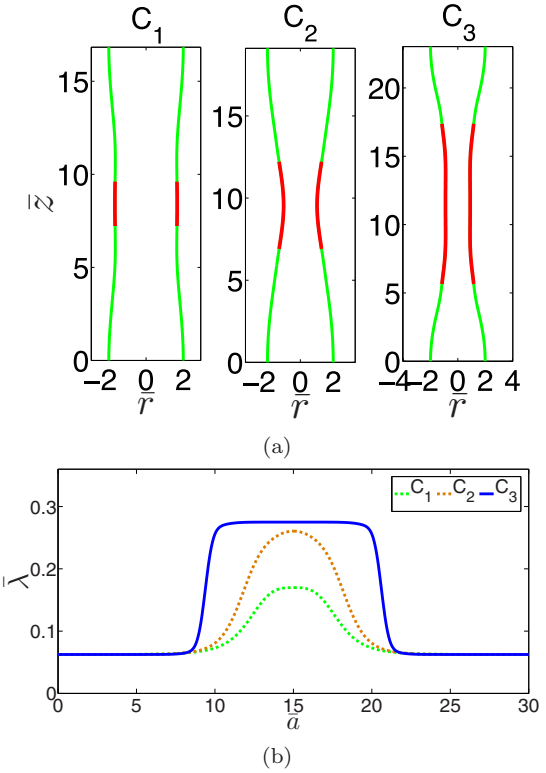

FIG. 5. (Color online) (a) Tubule shapes for the three concentration fields. The red curve is the protein-coated segment while the green curve is the uncoated segment. (b) Surface tension field for the three geometries.

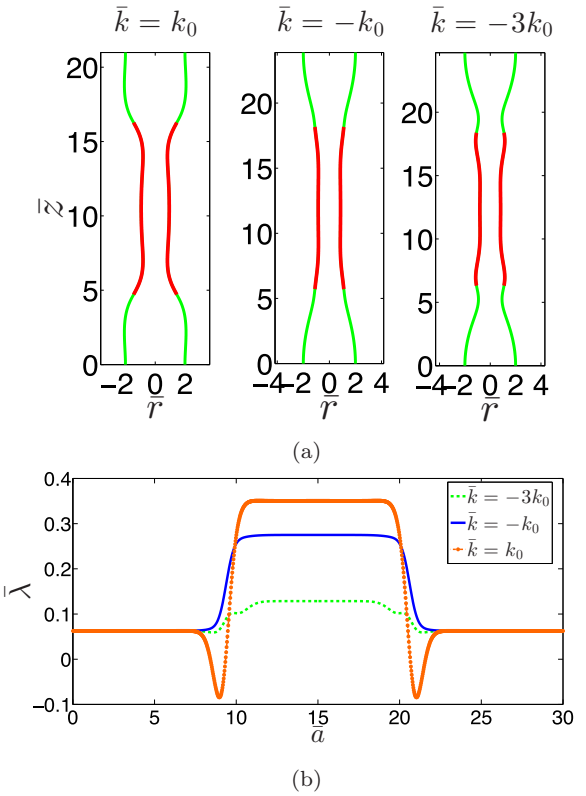

FIG. 6. (Color online) (a) Tubule shapes for the three prescribed Gaussian moduli for the C_3 concentration field. The red curve is the protein-coated segment while the green curve is the uncoated segment. (b) Surface tension field for the three geometries.

numerical data on an estimate of the Gaussian modulus in the protein-coated domain. If the modulus remains unaffected by the scaffold, which appears rather non-intuitive, the equilibrium equations and the boundary conditions remain unchanged and the results presented before hold. If the modulus changes spatially, like the other bending moduli, it would affect both the geometry and the membrane stresses. To get a quantitative insight into this effect, we revisit the tubule problem with a modified strain energy $\bar{W}(H,D,K;s) = W(H,D;s) + \bar{k}(s)[K - K_0(s)]$, where the first term is the energy in Eq. (44) and the second term is the contribution from the Gaussian curvature. Since crescent-shaped dimers prefer a cylindrical geometry, we set $K_0(s) = 0$. In the uncoated domain, we set $\bar{k} = -k_0$ based on the recent findings of Hu *et al.* [43]. In the protein-coated domain, we perform a parametric analysis and compute the equilibrium solution for a few different values of $\bar{k}$. A similar approach was adopted by Das *et al.* to model the impact of Gaussian modulus on the geometry of a membrane with two distinct phases of lipids [44]. Since the constraint on the Gaussian modulus from the stability condition is not known for anisotropic membranes at present, we allow the modulus to span both the positive and the negative regimes. The tubule shapes and the membrane tension variations for three specific values of maximum $\bar{k}$ ($\bar{k} = k_0, -k_0, -3k_0$) corresponding to the C_3 concentration field are shown in Fig. 6. The changes in the overall geometry are rather subtle with minor variations occurring near the membrane-coat interface. The changes in the membrane tension, however, appear more significant, especially for the positive value of the modulus. Overall, the variations in the Gaussian modulus do not alter the qualitative response of the tubule.

V. CONCLUSION

We have derived the generalized theory for lipid membranes that interact with protein scaffolds inducing anisotropic spontaneous curvatures. In addition to the mean curvature and Gaussian curvature, the strain energy for a membrane interacting with a protein scaffold with orthotropic symmetry depends on the curvature deviator. Inclusion of this invariant alters both the equilibrium equations and the edge conditions as shown in this paper. The proposed theory is equipped to model various kinds of spatial heterogeneities that may arise because of the membrane-protein interactions. We show the efficacy of the theory by modeling the squeezing of a tubule by crescent-shaped proteins. We emphasize the role of the equilibrium equation in the tangential plane by evaluating the surface tension field on the surface and showing its nonuniform behavior. Since membrane tension is a critical component in several cellular processes and remains an enigma in experimental studies, modeling-based quantitative estimates of tension can prove to be of vital importance. We model the influence of the Gaussian modulus on the equilibrium geometry and the membrane tension. Although the influence of the protein coat on the modulus is unknown at present, a

comparison of the experimental data on tubule shapes with the simulation results might provide an avenue to gain insight into the nature of the modulus.

Overall, the proposed framework would be valuable in comprehending biological phenomena where membrane-protein scaffold interactions play an important role. This bears special relevance for modeling of endocytic pathways in yeast and mammalian cells as cylindrical protein coats play a critical role in both vesicle formation and fission. Lack of an apt mathematical framework may lead to erroneous conclusions about the need and roles of different components of the endocytic machinery. In addition, the proposed framework would form the basis for formulating a dynamic model to capture the self-assembly of such proteins on a curved surface. This would be critical for understanding curvature-based protein sorting and localization in cellular membranes.

ACKNOWLEDGMENT

The authors are grateful to Professor David Steigmann for stimulating discussions.

[1] D. Boal, *Mechanics of the Cell* (Cambridge University Press, Cambridge, 2002).
[2] B. Alberts, A. Johnson, J. Lewis, M. Raff, K. Roberts, and P. Walter, *Molecular Biology of the Cell*, 4th ed. (Garland Science, New York, 2002).
[3] R. Phillips, J. Kondev, J. Theriot, and H. G. Garcia, *Physical Biology of the Cell* (Garland Science, New York, 2013).
[4] P. D. Camilli and K. Farsad, Curr. Opin. Cell Biol. **15**, 372 (2003).
[5] H. T. McMahon and J. L. Gallop, Nature (London) **438**, 590 (2005).
[6] J. Zimmerberg and M. Kozlov, Nat. Rev. Mol. Cell Biol. **7**, 9 (2006).
[7] W. Helfrich, Z. Naturforsch. C **28**, 693 (1973).
[8] U. Seifert, K. Berndl, and R. Lipowsky, Phys. Rev. A **44**, 1182 (1991).
[9] Z. C. Ou-Yang, J. X. Liu, and Y. Z. Xie, *Geometric Methods in the Elastic Theory of Membranes in Liquid Crystal Phases* (World Scientific, Singapore, 1999).
[10] D. J. Steigmann, Arch. Ration. Mech. Anal. **150**, 127 (1999).
[11] J. T. Jenkins, SIAM J. Appl. Math. **32**, 755 (1977).
[12] B. J. Peter, H. M. Kent, I. G. Mills, Y. Vallis, P. Jonathan G. Butler, P. R. Evans, and H. T. McMahon, Science **303**, 495 (2004).
[13] A. Frost *et al.*, Cell **132**, 807 (2008).
[14] A. Frost, V. M. Unger, and P. D. Camilli, Cell **137**, 191 (2009).
[15] A. Shimada *et al.*, Cell **129**, 761 (2007).
[16] W. Helfrich and J. Prost, Phys. Rev. A **38**, 3065 (1988).
[17] V. K. Iglic, V. Heinrich, S. Svetina, and V. Zeks, Eur. Phys. J. B **10**, 5 (1999).
[18] V. K. Iglic, M. Remskar, G. Vidmar, M. Fosnaric, and A. Iglic, Phys. Lett. A **296**, 151 (2002).
[19] M. Fosnaric, K. Bohinc, D. R. Gauger, A. Iglic, V. K. Iglic, and S. May, J. Chem. Inf. Model. **45**, 1652 (2005).
[20] J. R. Frank and M. Kardar, Phys. Rev. E **77**, 041705 (2008).
[21] D. Kabaso, E. Gongadze, P. Elter, U. van Rienen, J. Gimsa, V. Kralj-Iglic, and A. Iglic, Mini Rev. Med. Chem. **11**, 272 (2011).
[22] A. Arkhipov, Y. Yin, and K. Schulten, Biophys. J. **95**, 2806 (2008).
[23] A. Arkhipov, Y. Yin, and K. Schulten, Biophys. J. **97**, 2727 (2009).
[24] Y. Yin, A. Arkhipov, and K. Schulten, Structure **17**, 882 (2009).
[25] G. S. Ayton, E. Lyman, and G. A. Voth, Faraday Discuss. **144**, 347 (2010).
[26] H. Cui *et al.*, Biophys. J. **104**, 404 (2013).
[27] G. S. Ayton, P. D. Blood, and G. A. Voth, Biophys. J. **92**, 3595 (2007).
[28] N. Ramakrishnan, P. B. Sunil Kumar, and J. H. Ipsen, Phys. Rev. E **81**, 041922 (2010).
[29] N. Ramakrishnan, P. B. Sunil Kumar, and J. H. Ipsen, Biophys. J. **104**, 1018 (2013).
[30] R. Bradley and R. Radhakrishnan, Polymers **5**, 890 (2013).
[31] T. Baumgart, B. R. Capraro, C. Zhu, and S. L. Das, Annu. Rev. Phys. Chem. **62**, 483 (2011).
[32] G. A. Holzapfel, *Nonlinear Solid Mechanics: A Continuum Approach for Engineering* (Wiley, New York, 2000).
[33] E. Kreyszig, *Differential Geometry* (University of Toronto Press, Toronto, 1959).
[34] Q. S. Zheng, Proc. R. Soc. London Ser. A **443**, 127 (1993).
[35] A. Agrawal and D. J. Steigmann, Biomech. Model. Mechanobiol. **8**, 371 (2009).
[36] A. Agrawal and D. J. Steigmann, Continuum Mech. Thermodyn. **21**, 57 (2009).
[37] W. Rawicz, K. C. Olbrich, T. McIntosh, D. Needham, and E. Evans, Biophys. J. **79**, 328 (2000).
[38] D. J. Steigmann, E. Baesu, R. E. Rudd, J. Belak, and M. McElfresh, Interface. Free Bound. **5**, 357 (2003).
[39] R. Capovilla and J. Guven, J. Phys.: Condens. Matter **16**, S2187 (2004).
[40] R. Capovilla, J. Guven, and J. A. Santiago, Phys. Rev. E **66**, 021607 (2002).
[41] Z. C. Tu and Z. C. Ou-Yang, Phys. Rev. E **68**, 061915 (2003).
[42] M. M. Müller, M. Deserno, and J. Guven, Phys. Rev. E **76**, 011921 (2007).
[43] M. Hu, J. J. Briguglio, and M. Deserno, Biophys. J. **102**, 1403 (2012).
[44] S. L. Das, J. T. Jenkins, and T. Baumgart, Europhys. Lett. **86**, 48003 (2009).